

Interactive Generalized Additive Model and Its Applications in Electric Load Forecasting

Linxiao Yang

linxiao.ylx@alibaba-inc.com
DAMO Academy, Alibaba Group
Hangzhou, China

Xinyue Gu

guxinyue.gxy@alibaba-inc.com
DAMO Academy, Alibaba Group
Hangzhou, China

Rui Ren

renrui.ren@alibaba-inc.com
DAMO Academy, Alibaba Group
Hangzhou, China

Liang Sun

liang.sun@alibaba-inc.com
DAMO Academy, Alibaba Group
Hangzhou, China

ABSTRACT

Electric load forecasting is an indispensable component of electric power system planning and management. Inaccurate load forecasting may lead to the threat of outages or a waste of energy. Accurate electric load forecasting is challenging when there is limited data or even no data, such as load forecasting in holiday, or under extreme weather conditions. As high-stakes decision-making usually follows after load forecasting, model interpretability is crucial for the adoption of forecasting models. In this paper, we propose an interactive GAM which is not only interpretable but also can incorporate specific domain knowledge in electric power industry for improved performance. This boosting-based GAM leverages piecewise linear functions and can be learned through our efficient algorithm. In both public benchmark and electricity datasets, our interactive GAM outperforms current state-of-the-art methods and demonstrates good generalization ability in the cases of extreme weather events. We launched a user-friendly web-based tool based on interactive GAM and already incorporated it into our eForecaster product, a unified AI platform for electricity forecasting.

CCS CONCEPTS

• **Computing methodologies** → **Machine learning algorithms.**

KEYWORDS

electric load forecasting, generalized additive model, interpretability, piecewise linear function

ACM Reference Format:

Linxiao Yang, Rui Ren, Xinyue Gu, and Liang Sun. 2023. Interactive Generalized Additive Model and Its Applications in Electric Load Forecasting. In *Proceedings of the 29th ACM SIGKDD Conference on Knowledge Discovery and Data Mining (KDD '23)*, August 6–10, 2023, Long Beach, CA, USA. ACM, New York, NY, USA, 11 pages. <https://doi.org/10.1145/3580305.3599848>

Permission to make digital or hard copies of all or part of this work for personal or classroom use is granted without fee provided that copies are not made or distributed for profit or commercial advantage and that copies bear this notice and the full citation on the first page. Copyrights for components of this work owned by others than the author(s) must be honored. Abstracting with credit is permitted. To copy otherwise, or republish, to post on servers or to redistribute to lists, requires prior specific permission and/or a fee. Request permissions from permissions@acm.org.
KDD '23, August 6–10, 2023, Long Beach, CA, USA

© 2023 Copyright held by the owner/author(s). Publication rights licensed to ACM.
ACM ISBN 979-8-4007-0103-0/23/08...\$15.00
<https://doi.org/10.1145/3580305.3599848>

1 INTRODUCTION

The electric load forecasting (ELF) [29] aims to predict future electricity consumption with historical observation data and other external factors such as numeric weather prediction (NWP). ELF is an indispensable procedure for the planning of power system industry [1] to meet the demand and supply equilibrium, as the decision-making process counts heavily on load prediction. With extreme weather events becoming more common, however, it is challenging to model the electricity demand patterns and to provide accurate predictions. A prediction too conservative can result in the threat of blackouts, whereas an aggressive prediction will make surplus electricity accrue, which can be a big waste particularly for non-regeneration energy. For example, California Independent System Operator (CAISO) found out that under-scheduling of demand by around 4.5% in the day-ahead market is the primary root cause for its proactive triggering of rotating blackouts in August 2020. A load forecast error of 1% in terms of mean absolute percentage error (MAPE) can turn into several hundred thousand dollars expenditure per GW peak for a utility's net income [23], let alone the inconvenience brought to the society.

Accurate electric load forecasting is challenging when there is limited data, such as load forecasting in holiday, or under extreme weather conditions (e.g., high temperature, cold wave, typhoon). These scenarios rarely happen but potentially have serious consequences and therefore draw tremendous attention of the power industry and the public sector. This problem becomes even more challenging when there is no training data. For example, given a record breaking high temperature in summer, the electric load also increases significantly. As there is no historical data with such high temperature, many machine learning models, including the popular decision tree ensemble methods, fail to make accurate prediction in this case.

In the traditional electric power industry, generally human experts use the results predicted by ELF for further usage in different applications, e.g., capacity planning and network planning [1]. As the human is in the loop, the interpretability of the forecasting model is crucial for the adoption of ELF models, especially when the prediction of ELF models and human experiences are inconsistent. Considering the nature of high-stakes decisions based on ELF, it is important to explain the model why it has reached a particular numerical result of predictions. Then experts are able to verify predictions so as to fine-tune models, troubleshoot or gain newer

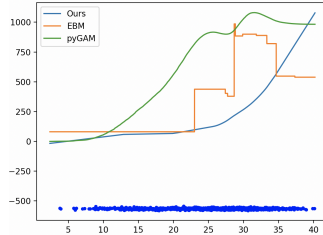


Figure 1: Existing GAMs (green line and orange line) fail to extrapolate at rightmost scenarios when examples are limited, whereas our interactive GAM (blue line) finds the monotone pattern (see Section 5.2 for details).

insights. Vice versa, human’s domain knowledge should also be incorporated into forecasting models. Translating knowledge into mathematical language is necessary to integrate prior knowledge or human supervision into the learning process. As [44] remarked that, interpretability allows human-machine collaboration and eventually leads to better performance.

Among these interpretable machine learning models, the Generalized Additive Model (GAM) has been particularly successful for dealing with large datasets and elucidating complex relationships [44]. GAM is clearly interpretable because the model is a linear combination of univariate component functions. It reveals the contribution and the effect of a single factor to the prediction by plotting a curve of the target variable as a function of each component. Besides interpretability, GAM has two other significant benefits for ELF. In practice, it not only yields accuracy as competitive as other sophisticated machine learning models [25, 52], but also fast to compute and therefore easy to deploy in industry. Thus, we choose to leverage GAM to develop our human-machine interactive ELF model in this study.

There could be some drawbacks of GAM in the context of ELF. First, the challenge of tackling with extreme conditions still remains unsolved. We conduct an experiment to demonstrate this phenomenon (detailed settings will be introduced in Section 5.2). As the result in Figure 1 shows, when the temperature climbs to an unprecedentedly high level (dots at bottom indicates frequency of such occurrences), two popular GAM algorithms, EBM [37] and PyGAM [45], are overwhelmed by the limited data, and make stable or even decreasing predictions. Second, it cannot effectively absorb specific domain knowledge in electric power industry. Recently, an editable GAM [53] has been proposed, but it cannot handle the specific form of domain knowledge in ELF. For example, usually the load increases monotonically as temperature increases in summer. By incorporating this domain knowledge, our proposed interactive GAM outperforms EBM and PyGAM significantly, as illustrated in Figure 1.

In this paper, we propose a novel GAM as a prescription for ELF to circumvent the above challenges. Our contributions includes:

- (1) A new GAM based on piecewise linear functions. We conduct numerical experiments of both benchmark regression tasks and ELF tasks. With its excellent performance in limited data settings, our method shows great extrapolation ability which improves the forecasting performance that users care about most.
- (2) An interpretable ELF model. The proposed model can not only “tell” the key factors for electric load via visualization,

but also “hear” the domain knowledge from experts in the electric power industry. We show how interpretability could lead to significant gains in ELF performance through the experiments.

- (3) A user-friendly tool, which provides an interactive web-based user interface for GAM. In particular, this tool has been incorporated into our eForecaster [59] product, a unified AI platform including robust, flexible, and explainable machine learning algorithms covering major electricity forecasting applications. Along with eForecaster, this tool has been deployed and applied in several provinces of China.

2 RELATED WORK

In this section, we first review the current state-of-the-art algorithms for electric load forecasting (ELF), and then delve into the recent progress of GAMs with an emphasis of their applications in ELF.

Electric load usually involves nonlinear modeling and exhibits seasonal patterns that change over time due to factors like weather changes [52], the economy drifts and holiday effect [12]. The electricity demand data, compared to sales data, can be of greater granularity temporally and spatially [23]. Based on the popular Global Energy Forecasting Competition (GEFCOM) held in 2012, 2014 and 2017 [23–25], a series of competitions focusing on energy demand forecasting, the majority of the top-ranked solutions consider statistical machine learning methods [19], including Gradient Boosting Machines (GBM) and Generalized Additive Models. In particular, the gradient boosting decision tree (GBDT) [19] and its variants, including XGBoost [9], CatBoost [43], LightGBM [27]), have enjoyed tremendous popularity in the load forecasting community [26, 30, 49]. By converting the forecasting problem to a regression problem, GBDT can deal with seasonality as well as auto-correlation and its prediction achieves good performance most of the time. However, it is reported that GBDT cannot predict well at the high loads [3], possible due to the fact that high loads data points are under-represented and overlooked by the training process. Also, model extrapolation is tough for such tree-based ensemble learners [35] as regression tree usually assigns a constant for a split feature space. This feature makes it difficult to tackle with scenarios where extrapolation is required. To summarize, GBDT and its variants are good forecasting models most of the time, but they fail to handle forecasting under extreme weather conditions.

Due to the huge success of deep neural networks [18], forecasting algorithms based on neural networks have become more and more popular. In late 1990s, the Electric Power Research Institute sponsored a project to build a short-term load forecasting system based on neural networks [28]. The resulting products are still being used by many power companies today. Later, a large body of literature has developed and applied deep learning models including LSTM-RNN [21], RBM [31], CNN [57] and more recently, transformer-based network [10, 60]. Despite the strong fitting power, deep learning architectures often suffer from overfitting due to multiple layers [46] and not well-interpretable to human. In particular, deep learning models usually require a large amount of training data, which is especially challenging for periods with

extreme weather conditions where limited or even no training data is available.

Another popular method for electric load forecasting is the highly explainable Generalized Additive Model [20]. It is also one of the most successful methods used in the top-ranked solutions in GEFCOM2012, 2014 and 2017 competitions [17, 36, 48]. In real-world application of electric power system, GAM has been widely adopted mainly due to its good practical performance, especially in tackling with extreme weather conditions and volatile, fluctuating load. For example, projects sponsored by Australian Energy Market Operators [14, 15] have developed a modified semi-parametric version of GAM. An extension of GAM with LASSO and tensor product interactions have also demonstrated its power in forecasting South Africa data [48], making it a useful tool for system operators in power utility companies.

Compared to neural networks and gradient boosting algorithms, GAM is favored by the industry for the following reasons. First, it identifies and characterizes nonlinear regression effects [19] and is able to jump the accuracy hurdles. In certain scenarios in ELF, GAM outperforms other methods while retains simplicity [17]. Another attractive feature of GAM is its interpretability. GAM is simple enough for human experts to read each component of the model, recognize which the significant predictors are and how a GAM works [22]. Thus, the effect of each factor on the prediction can be visualized in a graph, based on which humans can work on the follow-up feedback, such as model-debiasing [50], or potentially, refining the under-fitting parts.

GAM can be trained using different types of components, such as splines [55], regression trees and tree ensembles [5]. Splines are inefficient in modeling higher order interactions as number of parameters explodes exponentially [33]. Tree-based methods fit the curve in a piecewise constant way. Fitting GAM often involves backfitting [20] or gradient boosting [16]. Recently, some variants of GAM are proposed for improved accuracy [32, 33, 40, 41], such as GA²M [33], FLAM [41]. However, these GAMs cannot handle electric load forecasting when data is limited, especially in scenarios under extreme weather conditions. GAM Changer [53], an editable GAM tool is proposed to help domain experts and data scientists to fix problematic patterns. Unfortunately, it cannot deal with specific patterns of electric load effectively. In particular, when one function is modified, other functions still remain the same, potentially magnifying the fitting error. In other words, it lacks flexibility to handle complicated scenarios in real-world applications.

3 PROBLEM FORMULATION

In ELF, the domain knowledge is usually regarded as “trend knowledge” or “curve shape knowledge”. For example, when the temperature increases from 30 °C to 41 °C, the urban electric load in summer also increases. The trend may also have increasing marginal effect. That is, 1 °C up leads to much more load increase at 36 °C than that at 34 °C. But when the temperature is too high (say above 41 °C, basically all air conditioners are already running), increasing temperature only leads to fewer load rising. Thus we can conclude that when the temperature is above about 27 °C and below about 41 °C, the load is convex with respect to temperature and when the temperature is above about 41 °C the electric load is

concave with respect to temperature. However, these experts generally can determine the curve shape of the electric load as some key factors change (e.g., temperature), but they cannot quantify exact load change given these factors in general.

Our interactive GAM translates domain knowledge into constraints. Specifically, let $\mathbf{x}_i \in \mathbb{R}^D$ and $y_i \in \mathbb{R}$ be a collection of D features and the electric load at time index i , respectively. Usually, \mathbf{x}_i includes weather prediction, time and electric load in history, etc. In GAMs, we formulate y_i as the summation of the individual effects of $\{x_i^d\}_{d=1}^D$, i.e.,

$$y_i \approx \sum_{d=1}^D f_d(x_i^d), \quad (1)$$

where x_i^d is the d th feature of \mathbf{x}_i , $f_d(\cdot)$ is the shape function of x_i^d .

To incorporate the domain knowledge, given a dataset $\{(x_i, y_i)\}_{i=1}^N$, we aim to solve the following problem by introducing constraints:

$$\min_{\{f_d\}} \sum_{i=1}^N w_i \left(y_i - \sum_{d=1}^D f_d(x_i^d) \right)^2 \quad \text{s.t. } f_d \in \mathcal{A}_d, d = 1, 2, \dots, D. \quad (2)$$

Here w_i denotes the weight of i th sample, \mathcal{A}_d denotes the set consists of all shape functions satisfying the constraints added by user. We note that although we write the constraints in the formulation stage, actually, these constraints are added in an interactive manner. In other words, the constraints are added after the model is trained, and once the constraints added, the model is adjusted to fit these constraints.

We discuss \mathcal{A}_d , the feasible set of constraints for the d th feature. After extensive discussion with experts in the electric power industry, we define four types of constraints to represent the domain knowledge:

- The monotone increasing constraint in some range;
- The monotone decreasing constraint at some range;
- Convex constraint in some range;
- Concave constraint in some range.

For example, the monotone increasing constraints ensure that the electric load is monotone increasing when one of several factors increases in some range. Note that the convex combination of two monotone increasing shape functions is also a monotone increasing function. This property also holds for monotone decreasing, convex, and concave constraints. Thus, \mathcal{A}_d is a convex set based on its definition. Later we will show that this critical property empowers us to develop efficient algorithm to learn a set of shape functions to satisfy these constraints.

As discussed in Section 1, a key challenge in electric load forecasting under extreme weather conditions is the lack of training data in the past. For example, how to forecast the electric load at 40 °C in a city given the highest degree in the history collected is 38 °C. Thus, good model generalization on out-of-range data is crucial. We observe that for the electric load forecasting problem, the trend of the affection of factors (e.g., temperature) is usually smooth. For instance, the raising of the temperature from 38 °C to 39 °C leads to 10MW electric load increasing in a city recently, then we can also assume that the increase of electric load when the temperature increases from 39 °C to 40 °C is also around 10MW given other factors remaining the same. Thus, by discussing with

domain experts and analyzing the historical data, we propose to restrict the shape function $f_d(\cdot)$ being piecewise linear.

4 INTERACTIVE GAM

This section discusses our proposed interactive GAM. We first introduce the proposed piecewise linear GAM and then describe how we enable the model to be interactive with end users.

4.1 Piecewise linear GAM

4.1.1 Overall Framework. Our piecewise linear GAM is learned in the boosting framework. Specifically, we update the shape function $f_d(\cdot)$ according to the fitting residual in each iteration. At the t th iteration, fitting residual $\{r_i^{(t)}\}_{i=1}^N$ is

$$r_i^{(t)} = y_i - \sum_{d=1}^D f_d^{(t-1)}(x_i^d), \quad (3)$$

where $f_d^{(t-1)}$ denotes the estimate of f_d at the $(t-1)$ th iteration. Here we make an innocuous assumption that the mapping from $\{x_i^d\}_{i=1}^N$ to $\{r_i^{(t)}\}_{i=1}^N$ can be approximated using a piecewise linear function g , i.e.,

$$g = \mathbf{PLA}(\{x_i^d\}_{i=1}^N, \{r_i^{(t)}\}_{i=1}^N, \{w_i\}_{i=1}^N), \quad (4)$$

where $\mathbf{PLA}(x, r, w)$ denotes the operator which approximates r using a piecewise linear function of x , and w denotes the weight of each sample.

In the boosting framework, at the t th iteration, we update $f_d^{(t)}(x)$ with

$$f_d^{(t)}(x) = f_d^{(t-1)}(x) + \mu g(x), \quad (5)$$

where $\mu > 0$ is the step size. As we iteratively add piecewise linear functions to f_d , we then can ensure the final output f_d to be a piecewise linear function.

We summarize our piecewise linear GAM in Algorithm 1.

Algorithm 1: Piecewise Linear GAM

Input: Training dataset $\{x_i, y_i\}_{i=1}^N$, sample weight $\{w_i\}_{i=1}^N$, stepsize μ , maximum iteration T

Output: Shape function $\{f_d\}_{d=1}^D$

Initialization: $f_d^{(0)} = 0 \quad \forall d = 1 \dots D$;

for $t \leftarrow 1$ **to** T **do**

for $d \leftarrow 1$ **to** D **do**

 Step 1: compute $\{r_i^{(t)}\}$ according to (3)

 Step 2: approximate the relationship between $\{x_i^d\}$ and $\{r_i^{(t)}\}$ according to (4)

 Step 3: update shape function $f_d^{(t)}$ according to (5)

end

end

REMARK 1. We ensure the smoothness of f_i by forcing $g(x)$ to be smooth, instead of forcing f_i as backfitting based methods do. After several rounds of boosting, one can still get an f_i with edges. Compared with backfitting based methods, our method is more flexible.

4.1.2 Piecewise linear approximation. We now introduce our piecewise linear approximation method. Given a dataset $\{(x_i, r_i, w_i)\}_{i=1}^N$, we approximate r_i via a piecewise linear function of x_i with weight w_i . This is equivalent to the following optimization problem:

$$\min_{g \in \mathcal{L}} \sum_{i=1}^N w_i (g(x_i) - r_i)^2, \quad (6)$$

where \mathcal{L} denotes the set of all possible piecewise linear functions. The problem of approximating data points via piecewise linear function has been studied for years [13, 34, 47]. In this paper, we assume g is a weighted combination of hinge functions, reverse hinge functions and a constant:

$$g(x) = c + \sum_l \phi_l h(x - \eta_l) + \sum_l \phi_l^r h^r(x - \eta_l), \quad (7)$$

where c is an unknown constant, $\{\eta_l\}$ denotes the respect parameters, and $\{\phi_l\}$ and $\{\phi_l^r\}$ denote the weight of each functions. The hinge function $h(x)$ and reverse hinge function $h^r(x)$ are defined as $\max(x, 0)$ and $-\min(x, 0)$, respectively. Note that the hinge function is already used to learn piecewise linear functions in the literature. For example, in multivariate adaptive regression splines (MARS) models [19], hinge function is used as the basis function.

To find the optimal $\{c, \eta, \phi, \phi^r\}$, we first restrict $\{\eta_l\}$ in a known finite set of size L . We form matrix $A^h \in \mathbb{R}^{N \times L}$, whose (i, l) th elements is $h(x_i - \eta_l)$, and matrix $A^r \in \mathbb{R}^{N \times L}$, whose (i, l) th elements is $h^r(x_i - \eta_l)$. Stacking $\{g(x_i)\}$ as a vector, we have $[g(x_1), \dots, g(x_N)]^T = A\mathbf{q}$, where

$$A = [1, A^h, A^r], \quad (8)$$

$\mathbf{1} \in \mathbb{R}^{N \times 1}$ is a vector whose all elements is one, and

$$\mathbf{q} = [c, \phi_1, \dots, \phi_L, \phi_1^r, \dots, \phi_L^r]^T \quad (9)$$

denotes the unknown parameters. Formally, finding the optimal piecewise linear approximation of $\{r_i\}$ can be formulated as the following optimization problem:

$$\min_{\mathbf{q}} \|\mathbf{W}^{\frac{1}{2}}(\mathbf{r} - A\mathbf{q})\|_2^2, \quad \text{s.t. } \|\mathbf{q}\|_0 \leq K, \quad (10)$$

where $\mathbf{W} \in \mathbb{R}^{N \times N}$ denotes a diagonal matrix whose (i, i) th entry equals to w_i , $\|\cdot\|_0$ is the ℓ_0 pseudo-norm that counts the number of nonzero entries in the vector, and the constraint in (10) restricts $g(x)$ be formed by at most K ($K \ll N$) constant, hinge or reverse hinge functions. We note that this constraint can significantly reduce the computational complexity.

To ensure the generalization of the proposed method, instead of directly solving the problem (10), we solve the following regularized problem:

$$\min_{\mathbf{q}} \frac{1}{N} \|\mathbf{W}^{\frac{1}{2}}(\mathbf{r} - A\mathbf{q})\|_2^2 + \lambda \|\mathbf{q}\|_2^2, \quad \text{s.t. } \|\mathbf{q}\|_0 \leq K, \quad (11)$$

where we add a ℓ_2 -norm regularization on \mathbf{q} to avoid the shape change of $g(x)$, and parameter λ controls the trade-off between the fitting error and ℓ_2 -norm of \mathbf{q} .

Note that problem (11) is a variant of the sparse regression problem. The sparse regression problem has motivated a flourishing line of work [54, 56, 58]. Greedy methods, such as orthogonal matching pursuit (OMP), are one of the most popular methods, due to their computational efficiency. In this paper, we extend OMP [39] to solve

(11). As the vector \mathbf{q} is sparse, once we can estimate the positions of nonzero elements of \mathbf{q} , we can find the optimal \mathbf{q} by solving a least squares problem. Here we find the nonzero positions of \mathbf{q} by their corresponding columns of matrix \mathbf{A} . Specifically, we maintain a set Γ (initially empty) and keep adding to Γ with the column index of \mathbf{A} that most reduces the objective value until the size of Γ equals to K . Define \mathbf{A}_Γ be a matrix that formed by set $\{\mathbf{a}_i | i \in \Gamma\}$, where \mathbf{a}_i denotes the i th columns of \mathbf{A} . At the k th iteration, let \mathbf{q}_Γ be the weight vector estimate with respect to \mathbf{A}_Γ . The fitting residual \mathbf{b} is

$$\mathbf{b} = \mathbf{r} - \mathbf{A}_\Gamma \mathbf{q}'.$$

Let (\mathbf{a}, q) be the pair of column of \mathbf{A} and its corresponding weight. At the k th iteration, we aim to find a pair of (\mathbf{a}, q) minimizing

$$g(\mathbf{a}, q) = \frac{1}{N} \|\mathbf{W}^{\frac{1}{2}}(\mathbf{b} - \mathbf{q}\mathbf{a})\|_2^2 + \lambda q^2. \quad (12)$$

Fixing \mathbf{a} , we can find optimal q that minimizing (12) is given as

$$q^* = \frac{\mathbf{b}^T \mathbf{W} \mathbf{a}}{\mathbf{a}^T \mathbf{W} \mathbf{a} + \lambda N}. \quad (13)$$

Substituting it into (12), we arrive at

$$g(\mathbf{a}, q^*) = \frac{1}{N} \mathbf{b}^T \mathbf{W} \mathbf{b} - \frac{\mathbf{b}^T \mathbf{W} \mathbf{a}}{\mathbf{a}^T \mathbf{W} \mathbf{a} + \lambda N}. \quad (14)$$

Then at the k th iteration, we only need to find an \mathbf{a} minimizing (14). Once the optimal \mathbf{a} is found, its index is added into Γ , and \mathbf{A}_Γ is updated as $\mathbf{A}_\Gamma = [\mathbf{A}_\Gamma, \mathbf{a}]$. Then the optimal weight \mathbf{q}_Γ can be updated by minimizing

$$\min_{\mathbf{q}_\Gamma} \frac{1}{N} \|\mathbf{W}^{\frac{1}{2}}(\mathbf{r} - \mathbf{A}_\Gamma \mathbf{q}_\Gamma)\|_2^2 + \lambda \|\mathbf{q}_\Gamma\|_2^2, \quad (15)$$

which is a least squares problem and its optimal solution is given as follows

$$\mathbf{q}_\Gamma^* = (\mathbf{A}_\Gamma^T \mathbf{W} \mathbf{A}_\Gamma + \lambda N \mathbf{I})^{-1} \mathbf{A}_\Gamma^T \mathbf{W} \mathbf{r}, \quad (16)$$

where \mathbf{I} denotes the identity matrix. Once K pairs of (\mathbf{a}, p) are estimated, we estimate \mathbf{q} by replacing the elements at positions in Γ of a zero vector by \mathbf{q}_Γ^* .

We summarize our piecewise linear approximation method in Algorithm 2.

Algorithm 2: the proposed Piecewise Linear Algorithm (PLA)

Input: Dataset $\{(x_i, r_i, w_i)\}_{i=1}^N$, threshold set $\{\eta_l\}_{l=1}^L$, trade-off parameter λ , maximum number of basis K .

Output: $g(x)$

Initialization: form matrix \mathbf{A} according to (8), $\mathbf{b} = \mathbf{y}$, and $\Gamma = \emptyset$;

for $k \leftarrow 1$ **to** K **do**

Step 1: $\gamma_k = \arg \max_{j \notin \Gamma} \frac{\mathbf{b}^T \mathbf{W} \mathbf{a}_j}{\mathbf{a}_j^T \mathbf{W} \mathbf{a}_j + \lambda N}$

Step 2: $\Gamma = \Gamma \cup \gamma_k$ and $\mathbf{A}_\Gamma = [\mathbf{A}_\Gamma, \mathbf{a}_{\gamma_k}]$

Step 3: compute \mathbf{q}_Γ^* according to (16)

Step 4: $\mathbf{b} = \mathbf{r} - \mathbf{A}_\Gamma \mathbf{q}_\Gamma^*$

end

Step 5: Generate $g(x)$ according to (7) with \mathbf{q}_Γ^*

REMARK 2. For better generalization, we add a ℓ_2 -norm regularization on \mathbf{p} , which penalizes the slope of the hinge functions. λ controls the trade-off between smoothness and fitting error. Large λ leads to small \mathbf{q} and more smooth $f_d(x)$. To reduce the search space, we use one λ for all the features. \mathbf{q} is also affected by the Frobenius norm of \mathbf{A} . To wipe the effect of the value ranges of features on the magnitude of \mathbf{A} , we normalize the features before training. Apart from regularization terms, we can regularize the objective by pairwise selection for hinge function and reverse hinge function. In this way, γ_k is determined by

$$\gamma_k = \arg \max_{j \notin \Gamma} \frac{\mathbf{b}^T \mathbf{W} \mathbf{a}_j^h}{(\mathbf{a}_j^h)^T \mathbf{W} \mathbf{a}_j^h + \lambda N} + \frac{\mathbf{b}^T \mathbf{W} \mathbf{a}_j^r}{(\mathbf{a}_j^r)^T \mathbf{W} \mathbf{a}_j^r + \lambda N}, \quad (17)$$

where \mathbf{a}_j^h and \mathbf{a}_j^r denote the j th column of \mathbf{A}^h and \mathbf{A}^r , respectively. The pairwise selection avoids only fitting a small number of data, which leads to model overfitting.

REMARK 3. We discuss the computational complexity of the proposed method. The main computational complexity of the proposed method is dominated by Step 1 and Step 3 in Algorithm 2. Step 1 evaluates all the possible thresholds with computational complexity $O(NL)$. For Step 3, although inverse operation is involved, \mathbf{q}_Γ^* can be estimated efficiently by solving following equation

$$(\mathbf{A}_\Gamma^T \mathbf{W} \mathbf{A}_\Gamma + \lambda N \mathbf{I}) \mathbf{q}_\Gamma^* = \mathbf{A}_\Gamma^T \mathbf{W} \mathbf{r}, \quad (18)$$

with computational complexity $O(K^2)$. In our experiments, K is set to a quite small number, e.g., 5. Thus, the main computational cost lies in Step 1. Since the more thresholds are considered, the more accurate the approximation is, we tend to select large L , which further increases the computational complexity. To reduce the computational complexity, in the next section, we propose an efficient algorithm which reduces the computational complexity of Step 1 to $O(N + L)$.

4.2 Efficient Algorithm

In this subsection we introduce an efficient algorithm to speed up the computation in Step 1 of Algorithm 2 by utilizing the special structure of the hinge function. Without loss of generality, we assume the dataset $\{(x_i, r_i, w_i)\}_{i=1}^N$ is sorted according to x_i such that $x_1 \leq x_2 \leq \dots \leq x_N$, $\{\eta_l\}$ are also sorted such as $\eta_1 \leq \eta_2 \leq \dots \leq \eta_L$, and η_l corresponding to \mathbf{a}_l^h (and \mathbf{a}_l^r). For the l th threshold η_l , let $l' (1 \leq l' \leq N)$ be the index such that $x_{l'-1} < \eta_l \leq x_{l'}$. Then $(\mathbf{a}_l^h)^T \mathbf{W} \mathbf{a}_l^h$ can be formulated as

$$\begin{aligned} (\mathbf{a}_l^h)^T \mathbf{W} \mathbf{a}_l^h &= \sum_{i \geq l'} w_i (x_i - \eta_l)^2 \\ &= \sum_{i \geq l'} w_i x_i^2 - 2w_i x_i \eta_l + w_i \eta_l^2 \\ &= \sum_{i \geq l'} w_i x_i^2 - 2\eta_l \sum_{i \geq l'} w_i x_i + \eta_l^2 \sum_{i \geq l'} w_i. \end{aligned} \quad (19)$$

Following from (19), the value of $(\mathbf{a}_l^h)^T \mathbf{W} \mathbf{a}_l^h$ is determined by η_l and the values of accumulating $w_i x_i^2$, $w_i x_i$ and w_i from l' to N . We note that for different l' s, we can share the value of the accumulated $w_i x_i^2$, $w_i x_i$ and w_i to reduce the computational complexity. The pseudo-code of computing $(\mathbf{a}_l^h)^T \mathbf{W} \mathbf{a}_l^h$ for all l' s is summarized in Algorithm 3. Specifically, in the first step of Algorithm 3, we find the change point for the hinge function with each threshold η_l . We then

accumulate the reversed $\{w_i x_i^2\}$, $w_i x_i$, and w_i for all the possible values of l' . In our implementation, this operation is performed efficiently by invoking Numpy built-in function “cumsum” with linear computational complexity. In the final step, we evaluate $(a_l^h)^T W a_l^h$ according to (19). The computation of $(a_l^r)^T W a_l^r$ can be implemented similarly.

Algorithm 3: Compute weighted norm

Input: Dataset $\{(x_i, r_i, w_i)\}_{i=1}^N$, threshold set $\{\eta_l\}_{l=1}^L$
Output: $\{(a_l^h)^T W a_l^h\}_{l=1}^L$
 Step 1: for each l , find l' such that $x_{l'-1} < \eta_l \leq x_{l'}$
 Step 2: reverse $\{x_i\}$ and $\{w_i\}$
 Step 3: $z^o = \text{cumsum}(\{w_i x_i^2\})$, $z^p = \text{cumsum}(\{w_i x_i\})$, and $z^w = \text{cumsum}(\{w_i\})$
 Step 4: for each l , $(a_l^h)^T W a_l^h = z_{l'}^o - 2\eta_l z_{l'}^p + \eta_l^2 z_{l'}^w$

Similar to $(a_l^h)^T W a_l^h$, $b^T W a_l^h$ can be formulated as

$$\begin{aligned} b^T W a_l^h &= \sum_{i \geq l'} w_i b_i (x_i - \eta_l) \\ &= \sum_{i \geq l'} w_i b_i x_i - w_i b_i \eta_l \\ &= \sum_{i \geq l'} w_i b_i x_i - \eta_l \sum_{i \geq l'} w_i b_i. \end{aligned} \quad (20)$$

We can also compute the accumulation of $w_i b_i x_i$ and $w_i b_i$ in advance to reduce the computational complexity. The Pseudo-code of efficiently computing weighted correlation $b^T W a_l^h$ is shown in Algorithm 4.

So far, we have shown how to compute $(a_l^h)^T W a_l^h$ and $b^T W a_l^h$ efficiently, which enables us to implement Step 1 in Algorithm 2 in linear time complexity. Note that the proposed methods not only reduce the computational complexity, but also reduce the space complexity by avoiding explicitly generating matrix $A \in \mathbb{R}^{N \times (2L+1)}$, which is space-consuming when N and L are large.

Algorithm 4: Compute weighted correlation

Input: Dataset $\{(x_i, b_i, w_i)\}_{i=1}^N$, threshold set $\{\eta_l\}_{l=1}^L$
Output: $\{b^T W a_l^h\}_{l=1}^L$
 Step 1: for each l , find l' such that $x_{l'-1} < \eta_l \leq x_{l'}$
 Step 2: reverse $\{x_i\}$, $\{b_i\}$, and $\{w_i\}$
 Step 3: $z^o = \text{cumsum}(\{w_i x_i b_i\})$ and $z^p = \text{cumsum}(\{w_i b_i\})$
 Step 4: for each l , $b^T W a_l^h = z_{l'}^o - \eta_l z_{l'}^p$

4.3 User Interaction

We first introduce how to impose the four types of constraints to represent the domain knowledge mathematically, and then introduce the web-based user interface which supports two types of operations, including data point importance adjustment and constraint imposing.

4.3.1 Imposing Constraints to GAM. Note that the feasible sets of these four types of constraints introduced in Section 3 are all convex. Recall the updating strategy of $f_d(x)$ shown in (5), we can treat the piecewise linear function $g(x)$ as the gradient of $f_d(x)$ and update $f_d(x)$ using gradient projection method to force $f_d(x)$ satisfying the desired constraints, i.e.,

$$f_d^{(t)}(x) = \alpha f_d^{(t-1)}(x) + (1 - \alpha) \mathcal{P}_d(f_d^{(t-1)}(x) + \mu g(x)), \quad (21)$$

where the projection operator $\mathcal{P}_d(f)$ projects f onto the feasible set of the constraints applied on the i th feature.

Without loss of generality, we next introduce how to project a function f to the feasible set of monotone increasing constraints. Let \mathbf{x} be a vector formed by the anchor points in the region of interest. We discuss how to find a monotone increasing vector \mathbf{x}' such that $\|\mathbf{x}' - \mathbf{x}\|$ is minimized. Formally, the vector \mathbf{x}' can be found by solving the following problem

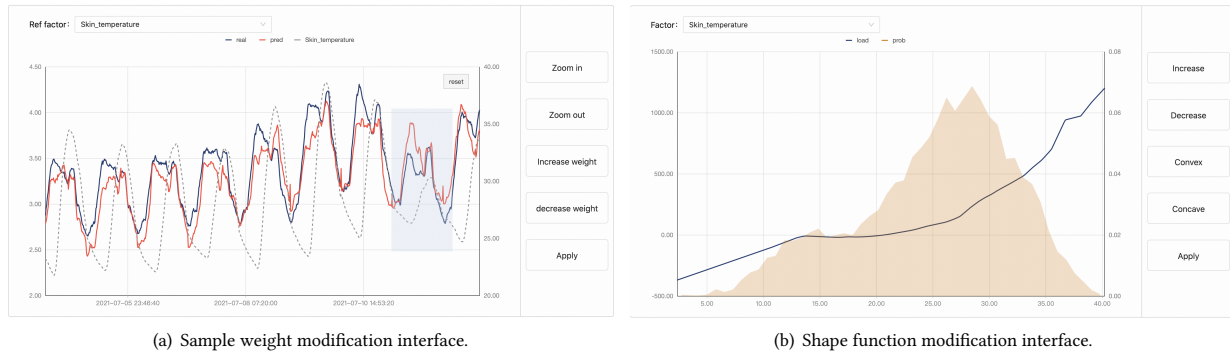
$$\min_{\mathbf{x}'} \|\mathbf{x}' - \mathbf{x}\|_2^2 \quad \text{s.t. } D\mathbf{x}' \geq \mathbf{0}, \quad (22)$$

where the matrix D is the differential matrix. Problem (22) can be solved by existing optimization methods, such as alternating direction multiplier methods (ADMM) [8]. Nevertheless, as the projection with quadratic complexity is invoked in every iteration, it is unpractical to repeat it. To speed up the computation, we devise an approximation algorithm. Specifically, \mathbf{x}' is set to be the average of the monotone increasing upper envelope and the lower envelope. If \mathbf{x} is already monotone increasing, our method will ensure $\mathbf{x}' = \mathbf{x}$, which is a key property of the projection operator.

The rest three constraints can be handled similarly. For monotone decreasing constraint, we reverse the vector, apply the monotone increasing approximation and then reverse it back. For convex constraints, we find a vector \mathbf{x}' , whose difference is monotone increasing. We approximate the difference of \mathbf{x} using our monotone increasing approximate method, and then accumulate it back to get the convex approximation. Similarly, concave constraints can be satisfied by forcing the difference of \mathbf{x} to be monotone decreasing.

4.3.2 User interface. For the convenience of experts with no experience in machine learning to incorporate domain knowledge into GAM, we develop a web-based user interface for our interactive GAM. The interface supports two types of operations.

The first type of operation adjusts the importance of the data points. In ELF, users usually care more about prediction under extreme weather events (such as extremely low or high temperature). They can ask the model to pay more attention to historical events with specific extreme weather conditions. To this end, our interactive GAM provides a sample weight modification interface, as shown in Fig.2(a). The weight modification interface plots the historical and the predicted electric load in “real” and “pred” lines, respectively (the scale of the load on the left is distorted due to data privacy). To increase the weight, the user only needs to select a segment of the lines and click the “Increase weight” button to upweight selected samples. Each button click will multiply the weights of the selected samples by 2. We also provide “Decrease weight” button for users to downweights certain outliers. After the weights are modified, users can click the button “Apply” to retrain the model. To help the user find similar events quickly, we also plot the value of the reference factors to indicate the type of



(a) Sample weight modification interface.

(b) Shape function modification interface.

Figure 2: User interface of our interactive GAM.

the extreme event in dash line, labeled as the factor name, such as “Skin_temperature”, with scale on the right. Users can select the reference factor from the drop down box named “Ref Factor”. As the extreme events rarely occur, we also provide “Zoom in” and “Zoom out” button to help the user search similar events over a long time range.

The second type of operation adjusts the GAM model by imposing the four types of constraints discussed in Section 3. We develop the shape function modification interface, as shown in Figure 2(b). The line in the main view is the shape function of the specified factor labeled as “load”, with its scale on the left. The shaded part labelled as “prob” is the data density that indicates how many data will be affected if constraints are added on this area, with its scale on the right. Users can first select a target region and choose an option from “Increase”, “Decrease”, “Convex” and “Concave” to impose monotone increasing, monotone decreasing, convex or concave constraints onto the selected area, respectively. The factor can be chosen from the drop down box named “Factor”. Multiple constraints can be applied on one or different shape functions. Once all the constraints are imposed, by clicking “Apply” button, both the model and the shape functions will be updated to satisfy the user-imposed constraints. Although constraints are only imposed on a fraction of shape functions, all the shape functions will be updated to minimize the fitting error.

5 EXPERIMENTS

5.1 Experiments on Public Benchmark Datasets

In this subsection, we evaluate our proposed method in benchmark regression tasks. Table 1 summarizes the selected 6 public datasets, including “Abalone” [2], “Ailerons” [4], “Boston Housing” [7], “Pole” [42], “Stock” [6] and “ComputerAct” [11].

Table 1: Statistics of public benchmark datasets.

Dataset	Size	Attributes	Data Source
Abalone	4177	8	UCI
Ailerons	13750	40	Rui Camacho
Boston Housing	506	13	UCI
Pole	15000	48	UCI
Stock	950	10	StatLib
ComputerAct	8192	22	DELVE

5.1.1 Experiment Setup. Three state-of-the-art GAM algorithms are compared, including EBM [38], pyGAM [45], and FLAM [40]. EBM¹ is a GAM based on boosted-tree, which assumes the shape functions of features are piecewise-constant. EBM learns the model by iteratively generating decision trees, where only one feature can be used for splitting at each tree. pyGAM² is a widely used python GAM package, where shape functions are modeled as low-order splines. Backfitting method is used to learn the parameters of the splines. FLAM³ is a convex optimization based method, where the shape function is represented as a piecewise constant function and Fused LASSO [51] is invoked to solve the problem. Throughout our experiments, we set $\lambda = 1$, $K = 7$, and $\mu = 0.1$. We turn off the interaction and bagging in EBM for fair comparison.

5.1.2 Evaluation. Mean square error (MSE) is used to evaluate performance:

$$\text{MSE} = \frac{1}{N} \sum_{i=1}^N (y_i - \hat{y}_i)^2, \quad (23)$$

where \hat{y}_i is the predicted value. For all experiments, we leverage 5-fold cross-validation and calculate the average MSE for the evaluation result. From Table 2, our algorithm outperforms other two algorithms in all 6 tasks, especially with enormous improvement (77%) on the Stock dataset.

We take “Stock” as an example to analyze why our model outperforms other algorithms. Figure 3 shows the three algorithm’s fitting results on the same testing dataset, with fitting gap marked by circles. Compared with Interactive GAM, EBM cannot well fit the peak and dip. We attribute the phenomenon to the limitation of piecewise constant. Unlike piecewise linear, piecewise constant will let a group of different feature values be the same result, which loses accuracy. Our inference can be verified through inspecting the marked red circles. EBM fits these areas with the same value, whereas in the groundtruth these values vary a lot. We also plot the shape functions of the first six features on dataset “Stock” learned by our method, as Figure 4 shows. Users can better understand the predicting mechanism of the model from the visualization of the shape functions.

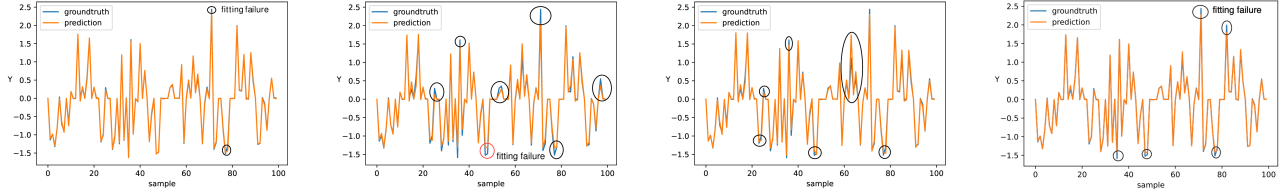
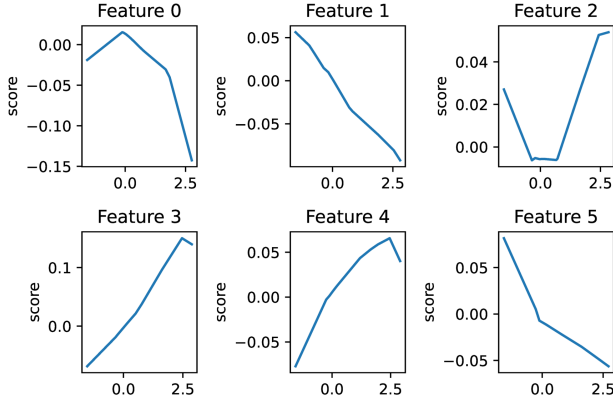
¹Code available at <https://github.com/interpretml/interpret>

²Code available at <https://github.com/dswah/pyGAM>

³Code available at <https://cran.r-project.org/web/packages/flam/>

Table 2: MSE of different algorithms on public benchmark datasets.

Model	Abalone	Ailerons	Boston Housing	Pole	Stock	ComputerAct
Ours	0.4164	0.1744	0.1402	458.8043	0.0026	0.02179
EBM	0.4729	0.1837	0.1656	460.5753	0.0114	0.02186
pyGAM	0.4272	0.1936	0.1582	464.1290	0.0142	0.02207
FLAM	0.4224	0.1822	0.2120	478.0053	0.0066	0.02206

**Figure 3: The predicting results on Stock dataset. From left to right: prediction obtained by our piecewise linear GAM, EBM, pyGAM, FLAM, respectively.****Figure 4: The shape functions of the proposed method learned on Stock dataset.****Table 3: RNMSE of different algorithms on the ELF dataset.**

Model	Ours	EBM	PyGAM	FLAM	recency
Overall	0.0859	0.0878	0.0893	0.0860	0.3645
Extreme event	0.0723	0.0736	0.0807	0.0937	0.0999

5.2 Experiments on Electric Load forecasting

In this subsection, we utilize a representative real-world electric load dataset to test the validity of our method. We also demonstrate how the experts can add domain knowledge to improve the performance of the model.

5.2.1 Electric Load Dataset. We collect the electric load data as well as the corresponding numerical weather prediction (NWP) of Henan province in China ranging from February 11, 2020 to July 25, 2022. We particularly focus on extreme weather events in summer, thus we only keep the data from May 1 to October 31 each year. The load data is recorded every 15 minutes, so there are 96 records a day. The sample size is 43488. The provincial NWP data is obtained from city-level averages. We use 6 key NWP features in prediction, including

surface pressure, surface sensible heat flux, total cloud cover, surface net solar radiation, total precipitation, and skin temperature⁴. In reality, if skin temperature is high for days (even if unchanged), then the electric load will increase gradually, known as “accumulating effect”. To model this effect, lagged features of skin temperature are generated. Apart from weather information, we also generate calendar- and solar-based features to capture the periodic property of the load. They are time-of-the-day, day-of-the-week, and month-of-the-year at the recorded time, respectively capturing the daily, weekly, and monthly cycles. We also generate features to indicate holiday effect. Lagged features of load are also generated as baseline reference. There are 18 features in total in the ELF dataset. We use the data before July 1, 2022 as training set and the rest as test set. We note that in July 14, 2022, Henan province suffers from extremely high temperature weather where the highest average skin temperature is above 40°C. We use the data on that day to measure the generalization ability under extreme weather events of each method.

5.2.2 Performance Evaluation. In addition to GAMs we compared above, we also consider a state-of-the-art ELF method, marked as “recency” [52], which models “recency effect” at an aggregated level. The “recency” method generates several features with power values of the temperature, and assumes that the electric load is linear in these features. Unlike GAMs that contain no interactions, the “recency” method includes a few of second order interactions. We set $\lambda = 0.1$, $K = 5$, $\mu = 0.05$ and $\alpha = 0.1$ for our method, and use default settings for the rest methods. We measure the performance of respective methods using root mean normalized square error (RNMSE):

$$\text{RNMSE} = \sqrt{\frac{1}{N} \sum_{i=1}^N \frac{(y_i - \hat{y}_i)^2}{y_i^2}}, \quad (24)$$

where \hat{y}_i denotes the predicted value.

⁴The detail meanings of these parameters can be found at <https://www.ecmwf.int/en/forecasts>

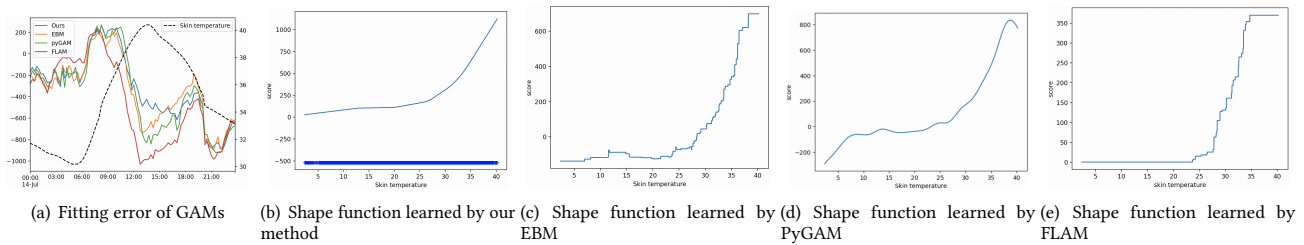


Figure 5: Fitting error and the shape functions of “Skin temperature” learned by respective GAMs.

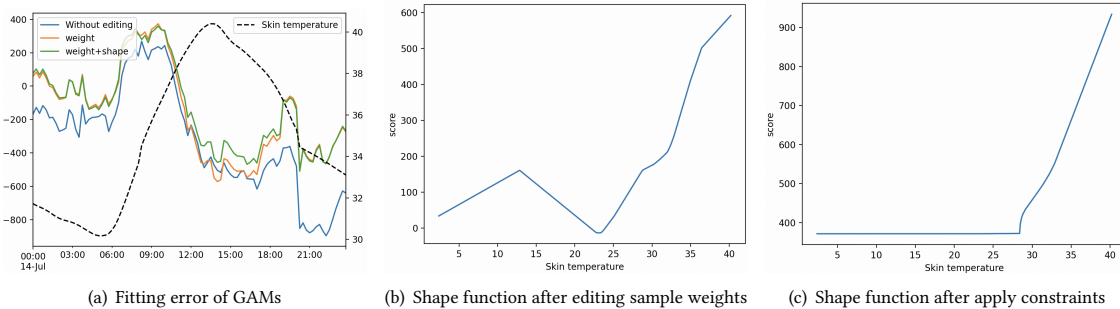


Figure 6: Fitting error and the shape functions of “Skin temperature” after editing our model.

In Table 3, our proposed method outperforms the rest in terms of RNMSE. To measure the generalization ability on extreme events, we also report the RNMSE on July 14, 2022, when extreme high temperature occurred, as Table 3 shows. Our proposed method reaches the lowest RNMSE when making this extrapolation. Figure 5(a) reports the fitting error, namely the gap between the predicted load and the true load on that day. All the methods have similar fitting error, except from 12:00 to 16:00, when the skin temperature is extremely high. Our proposed method produces fitting errors relatively closer to zero. Figure 5(b)-5(e) are the shape functions learned by GAMs. Although all the GAMs are able to discovery the trend that higher temperature leads to higher load, when the temperature is higher than 39°C , EBM, PyGAM and FLAM all fail to capture the increasing trend, which explains why our proposed method outperforms the rest during the time from 12:00 to 16:00.

Table 4: RNMSE of the proposed method before and after editing on extreme high temperature.

No editing	Edit weight	Edit weight + shape function
0.0723	0.0520	0.0475

5.2.3 Evaluation of Interactive Functions. To evaluate how performance is improved through our built-in interactive functions, we edit our model on extreme weather events using our user interface. We first select days with similar extreme events and perform the “increase weight” operation 16 times to retrain the model. In Figure 6(a), the orange line labeled as “weight” shows the fitting error after upweighting. From the figure we see that the fitting error before 3:00 and after 20:00 are significantly reduced. This is because the model pays more attention to the extreme events in history and is able to capture the the pattern of the load under

these extreme events. Table 4 reports that after upweighting, the RNMSE is reduced from 0.0723 to 0.0520. From Figure 6(b), it is worth noticing that as we put higher weight on the data with extremely high temperature, the shape function will fail to match the trend at low temperature. This issue can be fixed by restricting the curve from 0°C to 25°C to be monotone increasing. We apply the monotone increasing constraint and the re-updated model is further improved, as shown in Figure 6(a) with the green line labeled as “shape function + weight”. Table 4 implies that with more domain knowledge involved, the RNMSE is further reduced from 0.0520 to 0.0475, which is about 54% of the RNMSE of EBM. Meanwhile, the shape function successfully agrees with the experts’ domain knowledge in Figure 6.

6 CONCLUSION

In this paper, we propose an interactive GAM for electric load forecasting, allowing human experts to integrate domain knowledge in the model. While machine learning methods commonly overlook minority data such as extreme weather events and make unreliable extrapolations at out-of-the-box level, our method guarantees good performance within the range of factor values that users care about. We design an efficient algorithm to learn our interactive GAM composed of piecewise linear functions. The numerical results on public benchmark data and ELF data show that our method not only gives outperforming accuracy, but also extrapolates well at extreme factor levels and exhibits strong generalization ability. The method is proved to be practical in China, as users can easily refine the model with their expert knowledge by using the web-based interactive interface we deployed.

ACKNOWLEDGMENTS

This work was supported by Alibaba Group through Alibaba Research Intern Program.

REFERENCES

- [1] 2021. In *Intelligent Data-Analytics for Condition Monitoring*, Hasmat Malik, Nuzhat Fatema, and Atif Iqbal (Eds.). Academic Press, iv. <https://doi.org/10.1016/B978-0-323-85510-5.00012-0>
- [2] Abalone. 1995. Rui Camacho. <https://archive-beta.ics.uci.edu/dataset/1/abalone>
- [3] Raza Abid Abbasi, Nadeem Javaid, Muhammad Nauman Javid Ghuman, Zahoor Ali Khan, and Shujat Ur Rehman. 2019. Short term load forecasting using XGBoost. In *Web, Artificial Intelligence and Network Applications: Proceedings of the Workshops of the 33rd International Conference on Advanced Information Networking and Applications (WAINA-2019)* 33. Springer, 1120–1131.
- [4] Aileron. 1995. UCI Machine Learning Repository. <https://archive-beta.ics.uci.edu/dataset/1/aileron>
- [5] Eric Bauer and Ron Kohavi. 1999. An empirical comparison of voting classification algorithms: Bagging, boosting, and variants. *Machine learning* 36 (1999), 105–139.
- [6] Boston Housing. 1988. StatLib. <https://www.dcc.fc.up.pt/~ltorgo/Regression/stock.html>
- [7] Boston Housing. 1995. Delve Datasets. <https://www.cs.toronto.edu/~delve/data/boston/>
- [8] Stephen Boyd, Neal Parikh, Eric Chu, Borja Peleato, and Jonathan Eckstein. 2011. Distributed Optimization and Statistical Learning via the Alternating Direction Method of Multipliers. *Found. Trends Mach. Learn.* 3, 1 (jan 2011), 1–122.
- [9] Tianqi Chen and Carlos Guestrin. 2016. Xgboost: A scalable tree boosting system. In *Proceedings of the 22nd ACM SIGKDD international conference on knowledge discovery and data mining*. 785–794.
- [10] Weiqi Chen, Wenwei Wang, Bingqing Peng, Qingsong Wen, Tian Zhou, and Liang Sun. 2022. Learning to Rotate: Quaternion Transformer for Complicated Periodical Time Series Forecasting. In *Proceedings of the 28th ACM SIGKDD Conference on Knowledge Discovery and Data Mining*. 146–156.
- [11] ComputerActivity. 1995. Delve Datasets. <https://www.openml.org/search?type=data&sort=runs&id=197&status=active>
- [12] Henry A Dryar. 1944. The effect of weather on the system load. *Electrical Engineering* 63, 12 (1944), 1006–1013.
- [13] Claudia D'Ambrosio, Andrea Lodi, and Silvano Martello. 2010. Piecewise linear approximation of functions of two variables in MILP models. *Operations Research Letters* 38, 1 (2010), 39–46.
- [14] Shu Fan and Rob J Hyndman. 2011. Short-term load forecasting based on a semi-parametric additive model. *IEEE transactions on power systems* 27, 1 (2011), 134–141.
- [15] Shu Fan and Rob J Hyndman. 2012. Forecasting electricity demand in Australian national electricity market. In *2012 IEEE Power and Energy Society General Meeting*. IEEE, 1–4.
- [16] Jerome H Friedman. 2001. Greedy function approximation: a gradient boosting machine. *Annals of statistics* (2001), 1189–1232.
- [17] Pierre Gaillard, Yannig Goude, and Raphaël Nedellec. 2016. Additive models and robust aggregation for GEFCom2014 probabilistic electric load and electricity price forecasting. *International Journal of Forecasting* 32, 3 (2016), 1038–1050.
- [18] Ian J. Goodfellow, Yoshua Bengio, and Aaron Courville. 2016. *Deep Learning*. MIT Press, Cambridge, MA, USA. <http://www.deeplearningbook.org>.
- [19] Trevor Hastie, Robert Tibshirani, Jerome H Friedman, and Jerome H Friedman. 2009. *The elements of statistical learning: data mining, inference, and prediction*. Vol. 2. Springer.
- [20] Trevor J Hastie. 2017. Generalized additive models. In *Statistical models in S*. Routledge, 249–307.
- [21] Wan He. 2017. Load forecasting via deep neural networks. *Procedia Computer Science* 122 (2017), 308–314.
- [22] Stefan Hegselmann, Thomas Volkert, Hendrik Ohlenburg, Antje Gottschalk, Martin Dugas, and Christian Ertmer. 2020. An evaluation of the doctor-interpretability of generalized additive models with interactions. In *Machine Learning for Healthcare Conference*. PMLR, 46–79.
- [23] Tao Hong and Shu Fan. 2016. Probabilistic electric load forecasting: A tutorial review. *International Journal of Forecasting* 32, 3 (2016), 914–938.
- [24] Tao Hong, Pierre Pinson, and Shu Fan. 2014. Global energy forecasting competition 2012. , 357–363 pages.
- [25] Tao Hong, Jingrui Xie, and Jonathan Black. 2019. Global energy forecasting competition 2017: Hierarchical probabilistic load forecasting. *International Journal of Forecasting* 35, 4 (2019), 1389–1399.
- [26] Jing Huang and Matthew Perry. 2016. A semi-empirical approach using gradient boosting and k-nearest neighbors regression for GEFCom2014 probabilistic solar power forecasting. *International Journal of Forecasting* 32, 3 (2016), 1081–1086.
- [27] Guolin Ke, Qi Meng, Thomas Finley, Taifeng Wang, Wei Chen, Weidong Ma, Qiwei Ye, and Tie-Yan Liu. 2017. LightGBM: A Highly Efficient Gradient Boosting Decision Tree. In *Advances in Neural Information Processing Systems*, I. Guyon, U. Von Luxburg, S. Bengio, H. Wallach, R. Fergus, S. Vishwanathan, and R. Garnett (Eds.), Vol. 30. Curran Associates, Inc. <https://proceedings.neurips.cc/paper/2017/file/6449f44a102fde848669bdd9eb6b76fa-Paper.pdf>
- [28] Alireza Khotanzad, Reza Afkhami-Rohani, and Dominic Maratukulam. 1998. ANNSTLF-artificial neural network short-term load forecaster-generation three. *IEEE Transactions on Power Systems* 13, 4 (1998), 1413–1422.
- [29] Corentin Kuster, Yacine Rezugui, and Monjur Mourshed. 2017. Electrical load forecasting models: A critical systematic review. *Sustainable Cities and Society* 35 (2017), 257–270. <https://doi.org/10.1016/j.scs.2017.08.009>
- [30] Mark Landry, Thomas P Erlinger, David Patschke, and Craig Varrichio. 2016. Probabilistic gradient boosting machines for GEFCom2014 wind forecasting. *International Journal of Forecasting* 32, 3 (2016), 1061–1066.
- [31] Chengdong Li, Zixiang Ding, Dongbin Zhao, Jianqiang Yi, and Guiqing Zhang. 2017. Building energy consumption prediction: An extreme deep learning approach. *Energies* 10, 10 (2017), 1525.
- [32] Yin Lou, Rich Caruana, and Johannes Gehrke. 2012. Intelligible models for classification and regression. In *Proceedings of the 18th ACM SIGKDD international conference on Knowledge discovery and data mining*. 150–158.
- [33] Yin Lou, Rich Caruana, Johannes Gehrke, and Giles Hooker. 2013. Accurate intelligible models with pairwise interactions. In *Proceedings of the 19th ACM SIGKDD international conference on Knowledge discovery and data mining*. 623–631.
- [34] Alessandro Magnani and Stephen P Boyd. 2009. Convex piecewise-linear fitting. *Optimization and Engineering* 10 (2009), 1–17.
- [35] Hanna Meyer and Edzer Pebesma. 2021. Predicting into unknown space? Estimating the area of applicability of spatial prediction models. *Methods in Ecology and Evolution* 12, 9 (2021), 1620–1633.
- [36] Raphael Nedellec, Jairo Cugliari, and Yannig Goude. 2014. GEFCom2012: Electric load forecasting and backcasting with semi-parametric models. *International Journal of Forecasting* 30, 2 (2014), 375–381.
- [37] Harsha Nori, Samuel Jenkins, Paul Koch, and Rich Caruana. 2019. InterpretML: A Unified Framework for Machine Learning Interpretability. ArXiv. <https://www.microsoft.com/en-us/research/publication/interpretml-a-unified-framework-for-machine-learning-interpretability/>
- [38] Harsha Nori, Samuel Jenkins, Paul Koch, and Rich Caruana. 2019. InterpretML: A Unified Framework for Machine Learning Interpretability. *arXiv preprint arXiv:1909.09223* (2019).
- [39] Yagyensh Chandra Pati, Ramin Rezaifar, and Perinkulam Sambamurthy Krishnaprasad. 1993. Orthogonal matching pursuit: Recursive function approximation with applications to wavelet decomposition. In *Proceedings of 27th Asilomar conference on signals, systems and computers*. IEEE, 40–44.
- [40] Ashley Petersen and Daniela Witten. 2019. Data-adaptive additive modeling. *Statistics in medicine* 38, 4 (2019), 583–600.
- [41] Ashley Petersen, Daniela Witten, and Noah Simon. 2016. Fused lasso additive model. *Journal of Computational and Graphical Statistics* 25, 4 (2016), 1005–1025.
- [42] Pole telecommunication. 1995. UCI Machine Learning Repository. <https://www.dcc.fc.up.pt/~ltorgo/Regression/pole.html>
- [43] Liudmila Prokhorenkova, Gleb Gusev, Aleksandr Vorobev, Anna Veronika Dorogush, and Andrey Gulin. 2018. CatBoost: unbiased boosting with categorical features. *Advances in neural information processing systems* 31 (2018).
- [44] Cynthia Rudin, Chaofan Chen, Zhi Chen, Haiyang Huang, Lesia Semenova, and Chudi Zhong. 2022. Interpretable machine learning: Fundamental principles and 10 grand challenges. *Statistics Surveys* 16, none (2022), 1 – 85. <https://doi.org/10.1214/21-SS133>
- [45] Daniel Servén and Charlie Brummitt. 2018. pygam: Generalized additive models in python. *Zenodo*. doi 10 (2018).
- [46] Heng Shi, Minghao Xu, and Ran Li. 2017. Deep learning for household load forecasting—A novel pooling deep RNN. *IEEE Transactions on Smart Grid* 9, 5 (2017), 5271–5280.
- [47] Ali Siahkamari, Aditya Gangrade, Brian Kulis, and Venkatesh Saligrama. 2020. Piecewise linear regression via a difference of convex functions. In *International Conference on Machine Learning*. PMLR, 8895–8904.
- [48] Caston Sigauke. 2017. Forecasting medium-term electricity demand in a South African electric power supply system. *Journal of Energy in Southern Africa* 28, 4 (2017), 54–67.
- [49] Slawek Smyl and N Grace Hua. 2019. Machine learning methods for GEFCom2017 probabilistic load forecasting. *International Journal of Forecasting* 35, 4 (2019), 1424–1431.
- [50] Sarah Tan, Rich Caruana, Giles Hooker, and Yin Lou. 2018. Distill-and-compare: Auditing black-box models using transparent model distillation. In *Proceedings of the 2018 AAAI/ACM Conference on AI, Ethics, and Society*. 303–310.
- [51] Robert Tibshirani, Michael Saunders, Saharon Rosset, Ji Zhu, and Keith Knight. 2005. Sparsity and smoothness via the fused lasso. *Journal of the Royal Statistical Society: Series B (Statistical Methodology)* 67, 1 (2005), 91–108.
- [52] Pu Wang, Bidong Liu, and Tao Hong. 2016. Electric load forecasting with recency effect: A big data approach. *International Journal of Forecasting* 32, 3 (2016), 585–597.
- [53] Zijie J Wang, Alex Kale, Harsha Nori, Peter Stella, Mark E Nunnally, Duen Horng Chau, Mihaela Vorvoreanu, Jennifer Wortman Vaughan, and Rich Caruana. 2022. Interpretability, Then What? Editing Machine Learning Models to Reflect Human Knowledge and Values. In *Proceedings of the 28th ACM SIGKDD Conference on Knowledge Discovery and Data Mining*. 4132–4142.

- [54] Fei Wen, Lei Chu, Peilin Liu, and Robert C Qiu. 2018. A survey on nonconvex regularization-based sparse and low-rank recovery in signal processing, statistics, and machine learning. *IEEE Access* 6 (2018), 69883–69906.
- [55] Simon N Wood. 2003. Thin plate regression splines. *Journal of the Royal Statistical Society: Series B (Statistical Methodology)* 65, 1 (2003), 95–114.
- [56] John Wright, Yi Ma, Julien Mairal, Guillermo Sapiro, Thomas S Huang, and Shuicheng Yan. 2010. Sparse representation for computer vision and pattern recognition. *Proc. IEEE* 98, 6 (2010), 1031–1044.
- [57] Maheen Zahid, Fahad Ahmed, Nadeem Javaid, Raza Abid Abbasi, Hafiza Syeda Zainab Kazmi, Atia Javaid, Muhammad Bilal, Mariam Akbar, and Manzoor Ilahi. 2019. Electricity price and load forecasting using enhanced convolutional neural network and enhanced support vector regression in smart grids. *Electronics* 8, 2 (2019), 122.
- [58] Zheng Zhang, Yong Xu, Jian Yang, Xuelong Li, and David Zhang. 2015. A survey of sparse representation: algorithms and applications. *IEEE access* 3 (2015), 490–530.
- [59] Zhu Zhaoyang, Chen Weiqi, Xia Rui, Zhou Tian, Niu Peisong, Peng Bingqing, Wang Wenwei, Liu Hengbo, Ma Ziqing, Wen Qingsong, and Sun Liang. 2023. eForecaster: Unifying Electricity Forecasting with Robust, Flexible, and Explainable Machine Learning Algorithms. In *Thirty-Seventh AAAI Conference on Artificial Intelligence*. AAAI.
- [60] Tian Zhou, Ziqing Ma, Qingsong Wen, Xue Wang, Liang Sun, and Rong Jin. 2022. Fedformer: Frequency enhanced decomposed transformer for long-term series forecasting. In *International Conference on Machine Learning*. PMLR, 27268–27286.